Proceedings of the 17th International Heat Transfer Conference, IHTC-17
14 – 18 August 2023, Cape Town, South Africa

IHTC-17 | ID: 137

EFFICIENT MONTE CARLO RAY TRACING FOR APPARENT CAVITY BEHAVIOR

Ernest T. Lee, Ehsan Mofidipour, Matthew R. Jones, Brian D. Iverson*

Brigham Young University, Provo UT 84602, USA

ABSTRACT

Monte Carlo Ray Tracing (MCRT) is one common technique to characterize radiation exchange between surfaces. One MCRT algorithm approach considers the probability of each reflection, with non-reflected rays terminating (Forward MCRT). Here, the fraction of rays that are reflected are associated with the absorptivity of the surface. This approach generally requires a large ray count to provide a sufficient number of rays that survive multiple reflection events. In this work, we explore efficient MCRT approaches and pose additional computational methods that improve modeling efficiency to predict the apparent behavior of cavities. These efficient MCRT approaches include: uniformly distributed ray origins, use of the power absorption scheme, use of a Ray Count Power Series (RCPS), utilizing diffuse emission, and exploiting symmetry and boundary conditions.

Numerous ray origins for MCRT are required to adequately represent and span the origin surface. However, random assignment of these origins leads to long convergence times and significant computational effort to avoid clusters or voids of ray origins on an emitting surface. We show the use of distributed grids of emission points that avoid locally dense or sparse origins to reduce convergence time while providing low computational error. In particular, the introduction of a Ray Count Power Series (RCPS) in this work allows any intrinsic emissivity/absorptivity to be applied to the cavity interior surfaces in post-processing to obtain the apparent emissivity/absorptivity. The RCPS records the cumulative count of rays that experience a certain number of reflections within the cavity and is used to determine the apparent cavity emission/absorption for any intrinsic property using a single MCRT calculation. An alternative MCRT approach using a power absorption scheme that tracks the reduction of the radiative energy of each ray (as governed by the absorptivity of the surface) requires a lower ray count than traditional approaches as each ray is tracked through its entire path until the ray no longer interacts with the surfaces or cavity. The significance of simplifications such as symmetry and periodic boundary conditions on the number of traced rays is discussed. Finally, we show that Kirchhoff's Law also applies for apparent surfaces representing cavity openings, enabling the determination of radiative properties by equivalence. Methods provided in this work can be used to improve computational efficiency in MCRT modeling approaches with specific applications in apparent cavity behavior.

KEYWORDS: Ray Tracing, Radiation, Cavity Behavior, Thermal Management

1. INTRODUCTION

Monte Carlo ray tracing (MCRT) is one useful modeling approach for radiation heat transfer. This approach is a statistical method where a quantity of radiative energy is divided up and the fractions are assigned to numerous rays with magnitude and direction. The trajectory of the rays is tracked as they are reflected, transmitted, or absorbed at surfaces. When radiative heat exchange is modeled for complex surfaces or geometries (particularly when heat exchange occurs between multiple surfaces), Monte Carlo is a preferred modeling approach as the summation of rays over the hemisphere above a surface determines the net radiative flux for comparison with comparable black surface behavior. These quantities can then be used to calculate radiative surface properties [1].

Control of radiative surface properties is one way to control the absorption and emission of energy at a surface [2], [3]. Collapsible or origami-inspired surfaces offer the potential for dynamic control of radiative surface

*Corresponding Author: bdiverson@byu.edu

properties [4]–[9]. The expansion and contraction of V-groove-like cavities that comprise the surface allow for reconfigurable cavity geometries that will exhibit variable apparent radiative behavior (Fig. 1). As a surface collapses during folding, deep grooves are formed which trap radiative energy due to the high-aspect ratio cavity resulting in apparent radiative properties that approach the properties of a blackbody [4]. Similarly, as such surfaces expand, they exhibit radiative properties that are consistent with the intrinsic surfaces comprising the cavity. Actuation between these extremes results in the ability to dynamically alter the radiative heat exchange with the surface.

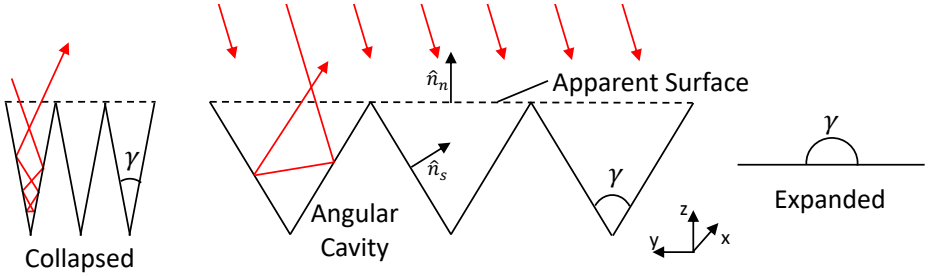

Fig. 1. Flow chart of the ray tracing algorithm. For the RCPS scheme, the ray tracer records the number of reflections each ray experiences. The power absorption scheme tracks the power of each ray absorbed by cavity surfaces.

MCRT is a powerful technique, especially when dealing with cavities whose internal surfaces may have spatial, angular, and spectral dependences. It has been applied to a variety of isothermal and non-isothermal arbitrarily-shaped cavities such as conical, spherical, cylindrical, and corrugated surfaces [10]–[15]. The basis of MCRT approximates geometric optics with no diffraction or near-field effects. One of the main concerns in using the MCRT method to compute radiative properties is computational time. Tracking and recording of emissions and direction of the incoming beams in either collision-based or pathlength methods requires a considerable amount of computational time. Reducing the computational time can be performed by evaluating the absorption coefficient of cavity surfaces [16].

In a computational sense, each ray originates at a specific location and is typically assumed not to interact with other rays, greatly simplifying the modeling. Such an approach also allows the rays to be modeled one at a time (or multiple rays through parallel computing) and summed to determine the net radiative behavior. This straightforward nature of MCRT has attracted researchers to use this method widely. Practices of MCRT have been documented in various publications [16]–[21]. The advantage of MCRT over other methods is that no prior knowledge for each geometry, such as view factors is necessary. The algorithm takes advantage of affordable computational cost and produces results without an in-depth study and derivation of each scenario.

MCRT offers the means to computationally determine the apparent radiative surface properties for dynamic, origami-inspired surfaces. As MCRT is a statistical approach intended to represent all possible variations of ray/surface interactions for a given scenario, many rays are typically required which can become computationally expensive. However, MCRT can introduce randomness in unnecessary aspects that slow the convergence of results. This work identifies techniques for cavity modeling that reduces randomness leading to efficiency in MCRT while also maintaining randomness in necessary aspects such as diffuse reflection. In particular, we address the efficient utilization of the following MCRT procedures to reduce computational effort: ray origin, power absorption scheme, Ray Count Power Series (RCPS), equivalent diffuse behavior, symmetry, boundary conditions, and equivalent models. These algorithms are particularly useful in efficiently obtaining apparent absorptivity across a wide range of intrinsic absorptivities.

2. RAY TRACING METHODOLOGY

Monte Carlo ray tracing is used to estimate the apparent radiative surface properties of angular cavities (e.g. Fig. 1). The ray tracing algorithm tracks the paths of rays to calculate the net absorption or emission of a cavity and determine the apparent radiative property exhibited by the cavity opening. Cavities can be considered to be ‘open’ when the cavities aren’t entirely enclosed by surfaces. However, MCRT may be performed on ‘closed’ cavities of a similar geometry where the cavity openings are replaced with an apparent surface (with apparent area A_a) used for ray counting and tracking of the cavity net behavior to the surroundings.

The ray tracing algorithm is essentially a loop that tracks rays emitted from interior cavity surfaces until they intersect with the apparent surface upon exiting (see example ray Fig. 1). This loop is schematically represented in Fig. 2. The ray tracer also calculates the point of intersection of the ray with cavity surfaces. Rays that intercept cavity surfaces can be considered to be absorbed or to impart energy according to the power absorption scheme (as described in section 3.2). When a ray is reflected, the direction of the reflected ray is calculated based on whether the reflection is diffuse or specular as specified by the specularity ratio (a quantity that defines the probability of a reflection being specular). This process of reflection and absorption repeats until the ray intercepts an exit surface, at which point the loop is terminated.

Ray tracing initialization begins by selecting the nature of the radiation (e.g., collimated irradiation or diffuse emission). Values are then assigned to the parameters involved in ray tracing including geometric parameters, actuation angle γ, intrinsic radiative surface properties (e.g., specularity ratio, intrinsic surface emissivity/absorptivity), and starting ray vectors.

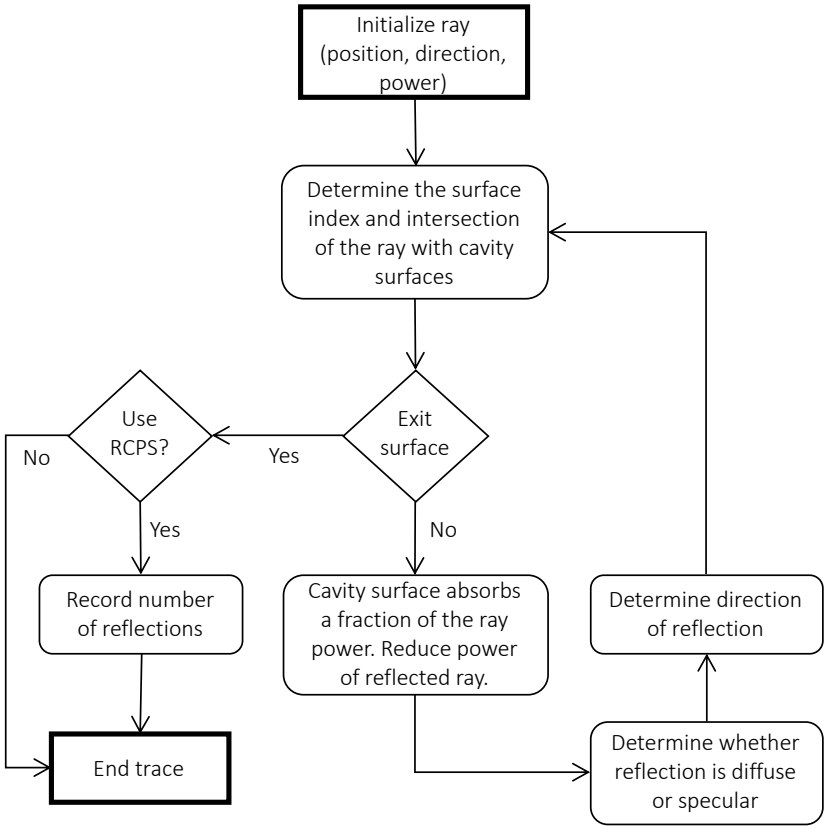

Fig. 2. Flow chart of the ray tracing algorithm. For the RCPS scheme, the ray tracer records the number of reflections each ray experiences. The power absorption scheme tracks the power of each ray absorbed by cavity surfaces.

Apparent directional emissivity (ε'_a) of an opaque, gray, and isothermal cavity is defined as the intensity of emitted and reflected (originating from emitting surfaces of the cavity) radiation exiting the cavity in a particular direction divided by the intensity of emitted and reflected radiation from a cavity of the same dimensions but comprised of black surfaces (Eq. 1). If the cavity's surfaces were intrinsically black, the apparent directional emissivity would equal unity in any direction where the apparent viewable area is nonzero.

$$\varepsilon'_a(\omega) = \frac{I_{e+r}(\omega)}{I_b(\omega)} \approx \varepsilon_i \frac{N'_{esc}(\omega)}{N'_{esc,b}(\omega)} \tag{1}$$

$I_{e+r}(\omega)$ specifies the radiative intensity emitted or reflected by a cavity that passes through an imaginary surface covering the cavity's opening within a differential solid angle dω centered on the direction ω. Prime notation is used here to indicate directional dependency.

In a computational sense, the ratio of intensities for directional emissivity can be approximated as the ratio of the number of rays exiting a real or black cavity into a particular small solid angle in a given direction. The intrinsic emissivity (ε_i) is included as a consequence of the decision to simulate the same number of rays generated from the intrinsic surfaces regardless of the intrinsic emissivity of the cavity. This apparent directional emissivity can be integrated over all directions to obtain an apparent spherical emissivity ($\varepsilon_a = \varepsilon_i \cdot N_{esc}/N_{esc,b}$). The word spherical is used to indicate the maximum range of the integration as the opening of a cavity may not necessarily be encompassed by a hemisphere unless the opening can be sufficiently captured by a single plane.

In a similar manner, the apparent directional absorptivity is defined as the incident intensity absorbed by the cavity from a particular direction divided by the total incident intensity in that direction, as follows.

$$\alpha'_a(\omega) = \frac{I_{i,abs}(\omega)}{I_i(\omega)} \approx \frac{N'_{i,abs}(\omega)}{N'_i(\omega)} \tag{2}$$

Again, this apparent directional absorptivity can be integrated over all directions to obtain an apparent spherical absorptivity ($\alpha_a = N_{i,abs}/N_i$). When using a power absorption scheme (as described in section 3.2), calculation of apparent RSPs may be performed by replacing ray counts (N and N') with hemispherical and directional power (P and P').

The MCRT created for this work was validated by comparing its results with the apparent absorptivity of a 3D V-groove for the conditions of approaching fully opened ($\gamma = 180°$), approaching fully closed ($\gamma = 0°$), and approaching infinite length (2D V-groove) [22]–[24]. As expected, when the 3D V-groove is fully opened, results show that the apparent absorptivity is equal to the intrinsic surface absorptivity. When the 3D V-groove approaches fully closed, the cavity appears black and the apparent absorptivity approaches unity. With increasing V-groove length, the solution converges to the 2D V-groove (infinite) solution. For 3D V-groove geometries, results indicate a maximum error of 0.05%, with the error presumably produced due to differing sample size and the stochastic nature of MCRT. These validation exercises give confidence in the algorithm of this work.

3. EFFICIENT RAY TRACING TECHNIQUES FOR CAVITIES

In ray tracing, where computational time and accuracy are often in competition, strategic and appropriate assumptions can save computational time while potentially increasing the accuracy of the results. In general, reducing randomness, which is often accommodated by increasing ray counts, can lead to efficient MCRT. The following methods provide a means to reduce randomness, avoid unnecessary redundancy and improve MCRT efficiency.

3.1. Ray Origin

Often, when determining ray origins, the origin locations are randomly assigned to the emitting surface. The number of rays is increased until the coverage of the emitting surface is sufficiently uniform. However, this approach can lead to a long convergence time due to random clusters and voids of ray origins on the emitting surface (Fig. 3a). One benefit to a random assignment of locations is that additional randomly assigned rays can be ‘added’ to the original set of randomly assigned locations in order to achieve ray count independence in the result.

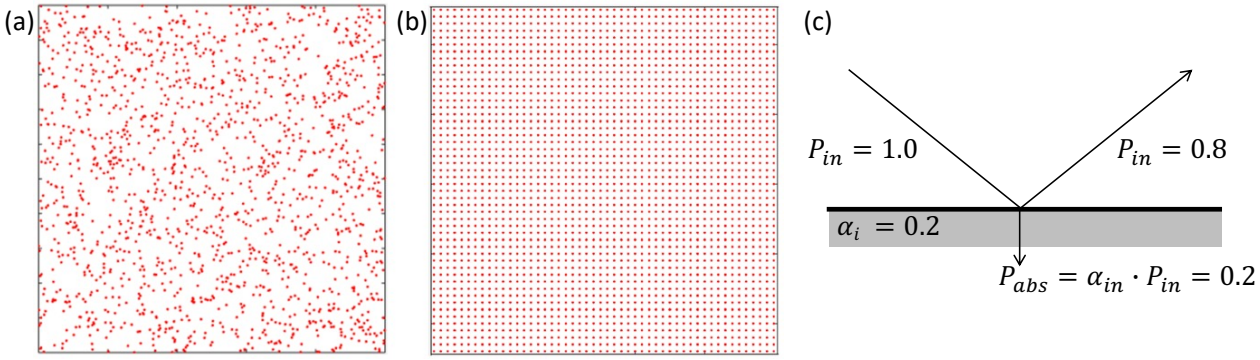

Fig. 3. (a) Randomly generated locations for the origin of rays resulting in a partially uniform distribution but with local clusters and voids which can contribute to longer convergence times. (b) Uniformly distributed points avoid the problem of clusters and voids, which can reduce convergence times. (c) Schematic illustrating rays with fractional power with an incoming ray that is partially absorbed resulting in a fraction of the initial ray energy being reflected. The amount absorbed is the product of the incoming power multiplied by the intrinsic absorptivity.

Alternatively, assigning a uniformly distributed set of ray origin locations to a grid would have no locally dense or sparse origins (Fig. 3b), leading to a shorter convergence time in general. However, if the uniformly distributed origin location density is insufficient to obtain a sufficiently low margin of error, the original set of ray origin locations would be discarded and the MCRT analysis would be rerun with a higher density (without the benefit of 'adding' data sets). In other words, if results from a 1000×1000 grid were insufficient to establish ray count independence, the results could not be added to results from a 2000×2000 grid for a combined result with higher accuracy. After determining a sufficient ray count that provides ray count independence in the desired result, a uniform ray origin assignment provides convergence at lower ray counts.

Time reduction can be illustrated by comparing the runtimes for a control case with a similar case using the improved algorithm under the same geometric and surface properties. Consider the case of determining the apparent hemispherical absorptivity of a 2D V-groove for $\gamma = 90°$. When specifying ray origin, the time reduction when using a uniform distribution is large when the sample size is small. Conversely, when a large amount of ray origin points are used, a random distribution vs. an ordered distribution exhibits little difference. Consider the case of a random distribution of 400 ray origin points; the number of simulations necessary to produce sets of results with a standard distribution of 0.01 is 126. However, the number of simulations using 400 ordered origin points that produces results with a standard distribution of 0.01 is 37. Further, as the number of ray origin points increases, the number of simulations required for a small standard distribution decreases for both ordered and random ray origin schemes, but the random scheme decreases more rapidly.

3.2. Power Absorption Scheme

A primary approach to modeling the transfer of energy at a surface associated with rays intersecting that surface is to do so statistically. Traditionally, the total number of rays incident on a surface would be reduced by the fraction of rays that are absorbed at that surface, as defined by the surface intrinsic absorptivity. If the number of possible reflections may be large (for a given geometry), then this approach may likely not be preferred. To have enough rays that continue through multiple absorption/reflection events, the total number of rays must be increased. This is particularly true for enclosure or cavity geometries, where multiple reflection events are anticipated.

An alternative method for transferring energy to a surface is to use a power absorption scheme. In this method, a fraction of the power associated with a given ray is absorbed by the surface (Fig. 3c). Each ray is traced through all absorption/reflection events as it intersects with the geometry, and the power in that ray is reduced following each absorption event. This method is generally superior to the typical MCRT approach where each ray is either fully absorbed or reflected as the power absorption scheme requires fewer rays for convergence. One drawback is that rays need to complete the same number of reflections as if the surfaces are completely reflective. As a result, a cavity with high intrinsic absorptivity will require as many reflections as a cavity with low intrinsic absorptivity. For very narrow cavities, this can significantly increase the computational time.

3.3. Ray Count Power Series

If the surfaces comprising a cavity have a uniform intrinsic emissivity and specularity ratio (r_s), the use of a ray count power series (RCPS, or matrix C) is a potentially superior approach to model rays with fractional power (as in the power absorption scheme). The ray count power series provides a cumulative count of rays that experience a certain number of reflections in a cavity composed of non-absorbing (perfectly reflecting) interior surfaces. Matrix C, comprised of the fraction of the total number of rays that experience one or more reflections, allows any intrinsic emissivity/absorptivity to be applied to cavity surfaces after tracing a sufficient number of rays and the intersection count of those rays with cavity surfaces is obtained. Therefore, once this RCPS has been obtained for perfectly reflecting interior surfaces, the apparent absorptivity or emissivity of a cavity for any intrinsic absorptivity or emissivity can be obtained without performing an MCRT analysis.

Apparent absorptivity/emissivity can be obtained as a weighted sum of the proportion of rays that experience a certain number of reflections.

$$\alpha_a = \sum_{n=1}^{\infty} C_n \cdot \alpha_i \cdot (1-\alpha_i)^{n-1} \tag{3}$$

For example, if 1000 rays were generated, where all rays were reflected at least once, 300 rays were reflected a second time, and no rays were reflected more than twice, then C = [1, 0.3, 0, ..., 0]. For a cavity comprised of surfaces with an intrinsic absorptivity (α_i) of 0.1, the apparent absorptivity of this cavity is obtained as follows: $[1 \times 0.1 \times (0.1^0)] + [0.3 \times 0.1 \times (0.1^1)] + 0 + \cdots + 0 = 0.127$. Since the values in matrix C do not increase from left to right, the apparent emissivity/absorptivity shown in Equation 3 must always increase and be concave down as the intrinsic emissivity/absorptivity increases from 0 to 1 (illustrated in Fig. 4). In addition, the apparent emissivity/absorptivity equals the intrinsic emissivity/absorptivity when the intrinsic properties are 0 or 1.

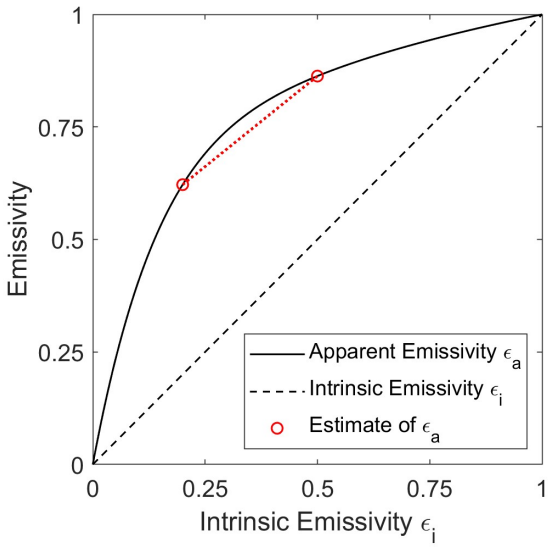

Fig. 4. Example relationship between apparent emissivity of an arbitrary cavity relative to the intrinsic emissivity of interior cavity surfaces.

Without the RCPS, if one were to calculate the apparent emissivity using MCRT at discrete values of intrinsic emissivity and interpolate between those values to determine the apparent emissivity at a different intrinsic emissivity (not calculated by MCRT), error would always be present in the interpolation (Fig. 4). However, as the RCPS enables determination of apparent emissivity in post processing using any desired intrinsic value, a continuous curve of all apparent absorptivities for a given cavity shape can be obtained using a single MCRT run using the RCPS. The RCPS reduces the complexity in obtaining all apparent emissivity values for a given geometry from O($n_s \times n_r$) to O(n_r), where n_s is the number of sample points of intrinsic emissivity, and n_r being the number of reflections in each run. Therefore, RCPS reduces the MCRT parameter space by one dimension as compared to the power absorption scheme. Since RCPS columns each represent a reflection, one consideration of using RCPS is that the RCPS will contain many columns for simulations with many reflections (such as a cavity with a small γ) and may occupy a large amount of memory.

3.4. Substitute Diffuse Emission

For the 2D V-groove, 3D V-groove (of finite length), and origami Miura-Ori tessellations [4], all interior cavity surfaces have the same tilt angle relative to the normal of the apparent surface representing the cavity opening, (i.e., $\hat{n}_s \cdot \hat{n}_n$ is the same for all surfaces, Fig. 1). For this condition, a cavity emitting diffusely can be simulated by irradiating the cavity from the normal direction while limiting the first reflection to be diffuse. Since the RCPS is defined above to track the proportion of absorbed rays, we alter the RCPS to reflect the proportion of apparent hemispherical emission in the following manner.

$$C_{hemis}[i] = \frac{C[i]-C[i+1]}{1-C[2]} = (C[i] - C[i+1])\frac{A}{A_a} \tag{4}$$

Equation 5 is an efficient method to obtain C_{hemis} for a cavity emitting diffusely, which can be obtained from matrix C for a cavity experiencing collimated irradiation along the normal to the apparent surface (aligned with the angle bisector of γ). After applying equation 5, the apparent hemispherical emissivity is obtained:

$$\varepsilon_a = \sum_{n=1}^{\infty} C_{hemis} \cdot \varepsilon_i \cdot (1-\varepsilon_i)^{n-1} \tag{5}$$

It is worth noting that the denominator $1 - C[2] = A_a/A = F_{i,a}$ is the view factor $F_{i,a}$ from the cavity to the apparent surface. For the 2D V-groove and Miura-Ori tessellations, the view factors happen to be $A_a/A = sin(\gamma/2)$. For Barretto's Mars tessellations [25], A_a/A is slightly more complicated but also has an analytical expression. For the 3D V-groove, where A_a is not simply a 2D planar surface, the view factor can be calculated using reference [26].

3.5. Symmetry

Symmetry is another method that can be used to significantly reduce the number of rays needed to model a given scenario. Usually, mirror or rotational symmetries are observed when dealing with 2D and 3D cavity configurations. For example, the 2D and 3D V-groove cavities have two mirror symmetries (XZ plane and YZ plane, Fig. 1). This means that the number of traces needed to obtain the full directional profile through collimated irradiation can be reduced by a factor of 1/4 in the azimuth direction from $0° \leq \phi \leq 360°$ to $0° \leq \phi \leq 90°$.

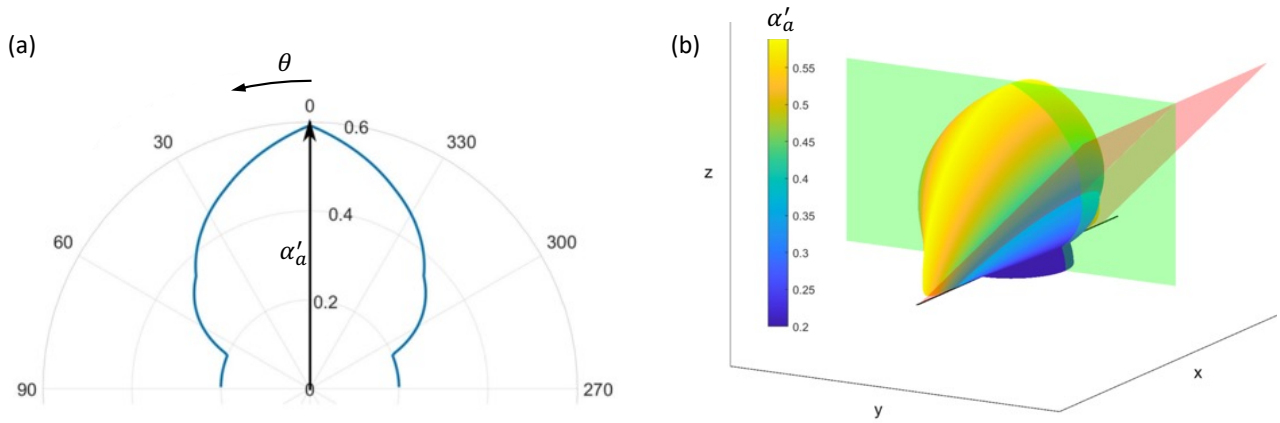

Fig. 5. (a) Directional absorptivity for a 2D V-groove cavity $\gamma = 45°$ and $\alpha_i = 0.2$. (b) 3D directional absorptivity for the 2D V-groove shown in part a. Note that the magnitude of $(\alpha'_a(\omega, \varepsilon_i))$ is constant along any arbitrary angled plane (pink) parallel to the x-axis. The cross-section along the YZ plane (green) is identical to that of part a.

In addition to mirror and rotational symmetries, another aspect of symmetry concerns the transformation from 2D emissivity/absorptivity directional properties to 3D ones. For a 2D geometry that extends along the x-axis infinitely, the x-component of the starting vectors does not affect the number of reflections. Fig. 5a illustrates the directional absorptivity of a 2D V-groove. However, Fig. 5b illustrates the 3D directional absorptivity of this 2D infinite V-groove. This means that the calculation of the directional emissivity/absorptivity profiles can be reduced from combinations of varying both θ and ϕ down to varying only θ at a fixed ϕ. For

convenience, this line is often chosen along the YZ plane at $\phi = 90°$. For example, if $\tan\theta_1 \cdot \sin\phi_1 = \tan\theta_2 \cdot \sin\phi_2$, symmetry along the x-axis means:

$$\alpha'_a(\theta_1, \phi_1) = \alpha'_a(\theta_2, \phi_2) \tag{6}$$

3.6. Boundary Conditions

Using mirror or periodic boundary conditions can simplify the model of the cavity radiative behavior. For example, a 2D V-groove can be modeled in a 3D environment as a 3D V-groove with the end surfaces of the cavity treated as mirrors [23]. However, when determining directional absorptivity, the mirror end surfaces may cause collimated rays entering the cavity to be reflected and continue in an incorrect direction, resulting in erroneous absorption characteristics. However, a periodic boundary condition can be applied to ensure collimated irradiation enters the cavity in the correct direction. Periodic boundary conditions can be applied when a pattern can be divided into repeating units with two identically shaped side surfaces, such as the repeating 3D patterns of the Miura Ori or Barreto's Mars tessellations. As a result of this periodic condition, only one unit cell needs to be modeled to represent the behavior of a surface comprised of many repeating unit cells.

3.7. Equivalent Properties

Kirchhoff's law for a surface states that the spectral, directional emissivity and absorptivity are equivalent ($\varepsilon'_\lambda = \alpha'_\lambda$). This condition is always applicable as they are inherent surface properties and independent of the spectral and directional distributions of the emitted and incident radiation [1]. Similarly, if the irradiation is diffuse or the surface is diffuse, the spectral, hemispherical emissivity equals the spectral, hemispherical absorptivity ($\varepsilon_\lambda = \alpha_\lambda$). Finally, if $\varepsilon_\lambda = \alpha_\lambda$ *and* one of the following conditions is satisfied, then the emissivity equals the absorptivity ($\varepsilon = \alpha$). Condition 1: the irradiation on a surface originates from a blackbody at the same temperature of the surface. Condition 2: the surface is gray and, therefore, independent of wavelength. Extensions of Kirchhoff's law are summarized in Table 2-2 of reference [27].

If $\varepsilon = \alpha$, only one of these properties needs to be calculated, and the more efficient modeling approach may be selected for convenience. In general, determining the apparent absorptivity of a cavity introduces less error than determining the apparent emissivity since the directions of the collimated irradiation can be controlled, whereas the direction of exiting rays from a cavity is randomized. For directional, apparent RSPs, it is therefore more efficient to calculate absorptivity with MCRT and obtain emissivity by equivalence.

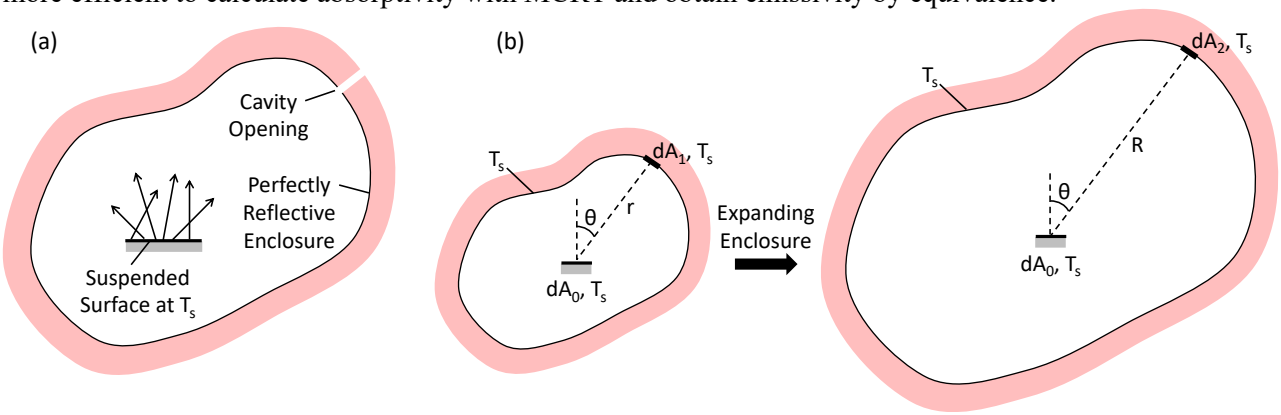

Fig. 6. (a) Generic cavity enclosure with a suspended surface at T_s. (b) Radiation exchange between the suspended surface and the isothermal enclosure as the enclosure expands.

Consider an evacuated enclosure comprised of perfectly reflecting interior surfaces (Fig. 6a). Within the enclosure is a suspended surface at T_s with non-zero intrinsic emissivity and in thermal equilibrium with the enclosure. Sufficient randomness in emission and reflection within the cavity results in diffuse radiation within the enclosure. The spectral radiosity of the cavity surfaces is greater than the spectral emissive power due to reflections. The spectral emissive power from a suspended surface is $\varepsilon_\lambda E_{\lambda,b}(T_s)A$. Since the enclosure is large and perfectly reflecting, the spectral irradiation on the suspended surface is diffuse. Therefore, the fraction of the emission from the suspended surface that is reflected by the suspended surface has a value of $\rho_\lambda \varepsilon_\lambda E_{\lambda,b} A$.

This reflected radiative power eventually returns to the suspended surface again since the enclosure is perfectly reflecting. Similarly, the fraction of the irradiation from the first reflection incident on the suspended surface has a value of $\rho_\lambda^2 \varepsilon_\lambda E_{\lambda,b} A$. Repeating this process, it is clear that as number of reflections goes to infinity (n→∞), the fraction of the radiative power reflected by the suspended surface is $\rho_\lambda^n \varepsilon_\lambda E_{\lambda,b}(T_s) A \approx 0$. In other words, all the spectral emissive power from the suspended surface is ultimately absorbed by the suspended surface after a large number of reflections. Therefore, the sum of the spectral radiative power leaving the surface (which, by definition, is the spectral radiosity of the surface) is given by.

$$J_\lambda A = \sum_{n=0}^{\infty} \rho_\lambda^n \varepsilon_\lambda E_{\lambda,b} A = \frac{\varepsilon_\lambda E_{\lambda,b} A}{1-\rho_\lambda} \tag{7}$$

However, since the incident spectral irradiation is diffuse, $\varepsilon_\lambda = \alpha_\lambda$ and

$$J_\lambda A = \frac{\varepsilon_\lambda E_{\lambda,b} A}{1-\rho_\lambda} = \frac{\varepsilon_\lambda E_{\lambda,b} A}{\alpha_\lambda} = E_{\lambda,b} A. \tag{8}$$

Based on this result, we see that the spectral radiation field within the enclosure is equal to the spectral emissive power of a blackbody regardless of the intrinsic properties of the suspended surface. In other words, the enclosure traps radiation within it, and the sum of the emitted and reflected radiative power is equal to the spectral emissive power of a blackbody. Since the suspended surface is the eventual destination of the blackbody radiation within the enclosure, we observe that the apparent absorptivity of the suspended surface is effectively unity.

Since the internal radiation characteristics are black, if a very small aperture is made to the enclosure (Fig. 6a), blackbody radiation at the steady state temperature T_s will be observed from the opening [1]. Since a blackbody radiation field exists within an isothermal cavity, the spectral intensity exiting a small opening in the cavity wall will equal $I_{\lambda,b}(T_s)$. This assumes the aperture is much smaller than the emitting, suspended surface in order to minimize disturbance to the equilibrium temperature. From the suspended surface's perspective, its surrounding has become isotropically black at temperature T_s. In other words, the shape of the enclosure cannot be observed by the suspended surface. Likewise, from anywhere within the enclosure, the suspended surface appears black and the shape of the suspended surface also cannot be observed.

Consider a section of the apparently black interior enclosure dA_1, which has zero net exchange of radiative power with the suspended surface dA_0, because the enclosure and suspended surface are in thermal equilibrium (see Fig. 6b). From an energy balance on the suspended surface, we observe the following.

$$P_{\lambda,0-1} = P_{\lambda,1-0} \tag{9}$$

From the perspective of the suspended surface, a steady state condition means that the radiative emission is equal to the absorption as follows.

$$\varepsilon_{\lambda,0-1} I_{\lambda,b} \frac{dA_0 dA_1 \cos\theta}{r^2} = \alpha_{\lambda,1-0} I_{\lambda,b} \frac{dA_0 dA_1 \cos\theta}{r^2} \tag{10}$$

For the scenario considered in Fig. 6b,

$$\varepsilon_{\lambda,0-1} = \alpha_{\lambda,1-0} \tag{11}$$

If the enclosure were to expand and become infinitely large while maintaining temperature T_s, $\varepsilon_{\lambda,0-1} = \alpha_{\lambda,1-0}$ remains true, resulting in a directional quantity as follows.

$$\varepsilon'_\lambda = \alpha'_\lambda \tag{12}$$

Note that there are no restrictions on the shape of the suspended surface or the relative direction of dA_0 or dA_1. Therefore, it can be concluded that Equation 6 ($\varepsilon'_\lambda = \alpha'_\lambda$) holds true in any direction without restrictions for any object in thermal equilibrium, including an apparent surface representing a cavity opening or $\varepsilon'_{\lambda,a} = \alpha'_{\lambda,a}$. Apparent versions of spectral hemispherical emissivity and absorptivity also are equivalent when the same

conditions required for equivalency for a nominally flat surface apply (i.e. diffuse irradiation). In a similar manner, apparent versions of total hemispherical emissivity and absorptivity are also equivalent (conditions 1 and 2 from above). Such equivalence of emissivity and absorptivity for apparent surfaces can readily be exploited to reduce the number of MCRT computations when calculating properties.

4. CONCLUSIONS

Monte Carlo ray tracing is a powerful computational tool used to model radiation exchange between surfaces as well as the net radiative behaviour of surfaces comprising a cavity. Cavity radiative behaviour can be consolidated into apparent surface properties (i.e. apparent emissivity and apparent absorptivity). Determination of these properties or the net cavity behaviour using MCRT requires tracking of a large number of rays and their intersections with cavity surfaces before they escape the cavity. As described in this paper, the computational effort is reduced by the following methods: uniformly distributed ray origins, use of the power absorption scheme, use of a ray count power series, utilizing diffuse emission, and exploiting symmetry and boundary conditions. In particular, the use of the ray count power series enables the determination of the apparent absorptivity/emissivity of a cavity for any intrinsic absorptivity/emissivity by performing the MCRT analysis. Additionally, we show that Kirchhoff's Law also applies for apparent surfaces representing cavity openings, enabling the determination of radiative properties by equivalence.

ACKNOWLEDGMENT

This material is based upon work supported by the National Science Foundation under Grant No. 1749395.

NOMENCLATURE

A	Area [m^2]	σ	Stefan Boltzmann constant (5.67×10^{-8} W m^{-2} K^{-4})
C	Ray count power series, RCPS (-)	θ	Elevation angle (°)
C_{hemis}	RCPS for diffuse emission (-)	ω	Solid angle or directional vector for θ and ϕ (°)
F	View factor (-)		
E	Emissive power (W m^{-2})	Subscripts and Superscripts	
G	Irradiation (W m^{-2})	$[]_a$	Indicates [] is an apparent quantity
I	Intensity (W m^{-2} μm^{-1} sr^{-1})	$[]_{abs}$	Indicates [] is absorbed
N_{esc}	Number of escaped rays (-)	$[]_b$	Indicates [] is for a blackbody
P	Power (W)	$[]_{e+r}$	Indicates [] emission and reflection
r	Distance (m)	$[]_i$	Indicates [] is from irradiation
T	Temperature (K)	$[]_s$	Indicates [] is a surface quantity
α	Intrinsic absorptivity (-)	$[]_\lambda$	Indicates [] is a spectral quantity
ε	Intrinsic emissivity (-)	$[]_0$	Indicates [] is for surface 0
ϕ	Azimuth angle (°)	$[]_1$	Indicates [] is for surface 1
ρ	Intrinsic reflectivity (-)	$[]'$	Indicates [] is a directional quantity

REFERENCES

[1] T. L. Bergman, A. S. Lavine, F. P. Incropera, and D. P. DeWitt, *Fundamentals of Heat and Mass Transfer*, 7th ed. Hoboken, NJ: Wiley, 2011.

[2] D. W. Hengeveld, M. M. Mathison, J. E. Braun, E. A. Groll, and A. D. Williams, "Review of modern spacecraft thermal control technologies," *HVAC and R Research*, vol. 16, no. 2, pp. 189–220, 2010, doi: 10.1080/10789669.2010.10390900.

[3] S. A. Hill, C. Kostyk, B. Motil, W. Notardonato, S. Rickman, and T. Swanson, "Thermal Management Systems Roadmap, Techology Area 14, April 2012," 2012.

[4] B. D. Iverson, R. B. Mulford, E. T. Lee, and M. R. Jones, "Adaptive net radiative heat transfer and thermal management with origami-structured surfaces," in *Proceedings of the 16th International Heat Transfer Conference, August 10-15, 2018*, Beijing, China, 2018.

[5] M. J. Blanc, R. B. Mulford, M. R. Jones, and B. D. Iverson, "Infrared visualization of the cavity effect using origami-inspired surfaces," *J Heat Transfer*, vol. 138, no. 2, 2016.

[6] R. B. Mulford, V. H. Dwivedi, M. R. Jones, and B. D. Iverson, "Control of Net Radiative Heat Transfer with a Variable-Emissivity Accordion Tessellation," *J Heat Transfer*, vol. 141, no. 3, 2019, doi: 10.1115/1.4042442.

[7] R. B. Mulford *et al.*, "Experimental demonstration of heat loss and turn-down ratio for a multi-panel , actively deployed radiator," *Appl Therm Eng*, vol. 178, no. January, p. 115658, 2020, doi: 10.1016/j.applthermaleng.2020.115658.

[8] R. B. Mulford, M. R. Jones, and B. D. Iverson, "Dynamic Control of Radiative Surface Properties With Origami-Inspired Design," *J Heat Transfer*, vol. 138, no. 3, 2016, doi: 10.1115/1.4031749.

[9] R. B. Mulford, M. R. Jones, and B. D. Iverson, "Heat transfer, efficiency and turn-down ratio of a dynamic radiative heat exchanger," *Int J Heat Mass Transf*, vol. 143, p. 118441, 2019, doi: 10.1016/j.ijheatmasstransfer.2019.118441.

[10] H. B. Su, R. H. Zhang, X. Z. Tang, and X. M. Sun, "Determination of the effective emissivity for the regular and irregular cavities using Monte-Carlo method," *Int J Remote Sens*, vol. 21, no. 11, pp. 2313–2319, 2000, doi: 10.1080/01431160050029594.

[11] R. B. Mulford, N. S. Collins, M. S. Farnsworth, M. R. Jones, and B. D. Iverson, "Total hemispherical apparent radiative properties of the infinite V-groove with specular reflection," *Int J Heat Mass Transf*, vol. 124, pp. 168–176, 2018, doi: 10.1016/j.ijheatmasstransfer.2018.03.041.

[12] Q. Fang, W. Fang, Z. Yang, B. X. Yu, and H. Hu, "A Monte Carlo method for calculating the angle factor of diffuse cavities," *Metrologia*, vol. 49, no. 4, pp. 572–576, 2012, doi: 10.1088/0026-1394/49/4/572.

[13] J. Wang, Z. Yuan, and Y. Duan, "Comparison of the emissivity uniformity of several blackbody cavities," in *AIP Conference Proceedings*, 2013, pp. 757–761. doi: 10.1063/1.4819637.

[14] J. De Lucas and J. J. Segovia, "Uncertainty calculation of the effective emissivity of cylinder-conical blackbody cavities," *Metrologia*, vol. 53, no. 1, pp. 61–75, 2016, doi: 10.1088/0026-1394/53/1/61.

[15] Y. Zhang, J. Dong, Z. Zhang, H. Sun, and G. Mei, "Circle vector function applied to ray tracing in MCM for calculating effective emissivities of blackbody cavities," *Infrared Phys Technol*, vol. 104, Jan. 2020, doi: 10.1016/j.infrared.2019.103104.

[16] B. N. Tomboulian and R. W. Hyers, "Predicting the effective emissivity of an array of aligned carbon fibers using the reverse monte carlo ray-tracing method," *J Heat Transfer*, vol. 139, no. 1, Jan. 2017, doi: 10.1115/1.4034310.

[17] J. R. Mahan, *Radiation Heat Transfer: A Statistical Approach*. New York, NY: John Wiley & Sons, 2001.

[18] Y. Zhao, J. Wang, G. Feng, and B. Cao, "Comparative Study on Radiation Properties of Blackbody Cavity Model Based on Monte Carlo Method," *Int J Thermophys*, vol. 41, no. 6, Jun. 2020, doi: 10.1007/s10765-020-02648-1.

[19] G. Mei, J. Zhang, X. Wang, S. Zhao, and Z. Xie, "Spectral and total effective emissivity of a nonisothermal blackbody cavity formed by two coaxial tubes," *Appl Opt*, vol. 54, no. 13, p. 3948, May 2015, doi: 10.1364/ao.54.003948.

[20] J. De Lucas and J. J. Segovia, "Uncertainty calculation of the effective emissivity of cylinder-conical blackbody cavities," *Metrologia*, vol. 53, no. 1, pp. 61–75, 2016, doi: 10.1088/0026-1394/53/1/61.

[21] S. He, C. Dai, Y. Wang, J. Liu, G. Feng, and J. Wang, "Analysis and improvements of effective emissivities of nonisothermal blackbody cavities," *Appl Opt*, vol. 59, no. 23, p. 6977, Aug. 2020, doi: 10.1364/ao.397229.

[22] R. B. Mulford, N. S. Collins, M. S. Farnsworth, M. R. Jones, and B. D. Iverson, "Total hemispherical apparent radiative properties of the infinite V-Groove with diffuse reflection," *J Thermophys Heat Trans*, vol. 32, no. 4, pp. 1108–1112, 2018, doi: 10.2514/1.T5485.

[23] R. B. Mulford, N. S. Collins, M. S. Farnsworth, M. R. Jones, and B. D. Iverson, "Total hemispherical apparent radiative properties of the infinite V-groove with specular reflection," *Int J Heat Mass Transf*, vol. 124, pp. 168–176, 2018, doi: 10.1016/j.ijheatmasstransfer.2018.03.041.

[24] B. D. Iverson, R. B. Mulford, E. T. Lee, and M. R. Jones, "Adaptive net radiative heat transfer and thermal management with origami-structured surfaces," in *Proceedings of the 16th International Heat Transfer Conference, August 10-15, 2018*, Beijing, China, 2018.

[25] T. A. Evans, R. J. Lang, S. P. Magleby, and L. L. Howell, "Rigidly foldable origami gadgets and tessellations," *R Soc Open Sci*, vol. 2, no. 9, Sep. 2015, doi: 10.1098/rsos.150067.

[26] D. C. Hamilton and W. R. Morgan, "Radiant-Interchange configuration factor," NASA TN 2836, 1952.

[27] J. R. Howell, M. Pinar Mengüç, K. Daun, and R. Siegel, “Thermal Radiation Heat Transfer: Seventh Edition,” 2020. doi: 10.1201/9780429327308.